

# 1 Chemical Control of Hydrodynamic Instabilities in Partially Miscible 2 Two-Layer Systems

3 M. A. Budroni,<sup>\*,†,§</sup> L. A. Riolfo,<sup>†</sup> L. Lemaigre,<sup>†</sup> F. Rossi,<sup>‡</sup> M. Rustici,<sup>¶</sup> and A. De Wit<sup>†</sup>

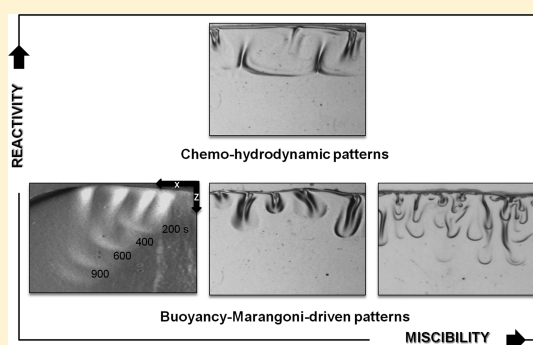
4 <sup>†</sup>Nonlinear Physical Chemistry Unit, Service de Chimie Physique et Biologie Théorique, Faculté des Sciences, Université Libre de  
 5 Bruxelles (ULB), CP231, 1050 Brussels, Belgium

6 <sup>‡</sup>Department of Chemistry and Biology, University of Salerno, via Ponte don Melillo, 84084 Fisciano, Salerno, Italy

7 <sup>¶</sup>Department of Chemistry and Pharmacy, University of Sassari, Via Vienna 2, Sassari 07100, Italy

8 **ABSTRACT:** Hydrodynamic instabilities at the interface between  
 9 two partially miscible liquids impact numerous applications, including  
 10 CO<sub>2</sub> sequestration in saline aquifers. We introduce here a new  
 11 laboratory-scale model system on which buoyancy- and Marangoni-  
 12 driven convective instabilities of such partially miscible two-layer  
 13 systems can easily be studied. This system consists of the stratification  
 14 of a pure alkyl formate on top of a denser aqueous solution in the  
 15 gravitational field. A rich spectrum of convective dynamics is obtained  
 16 upon partial dissolution of the ester into the water followed by its  
 17 hydrolysis. The properties of the convective patterns are controlled  
 18 by the miscibility of the ester in water, the feedback of the dissolved  
 19 species on its own miscibility, as well as the reactivity of given  
 20 chemicals in the aqueous solution with the solubilized ester.

21 **SECTION:** Liquids; Chemical and Dynamical Processes in Solution



22 **T**he study of buoyancy-driven convective mixing of partially  
 23 miscible fluids has recently gained renewed interest  
 24 because this process is at the heart of CO<sub>2</sub> sequestration  
 25 techniques, in which supercritical CO<sub>2</sub> is injected into  
 26 underground aquifers or petroleum reservoirs. After injection,  
 27 the CO<sub>2</sub> rises up to the impermeable cap rock, forming a layer  
 28 of less dense liquid on top of the denser brine or alkanes in  
 29 which it partially dissolves. The denser layer of dissolved CO<sub>2</sub>  
 30 then starts to sink into the lower liquid because of a buoyancy-  
 31 driven instability favoring further dissolution and mixing.<sup>1,2</sup>  
 32 Chemical reactions can affect this dissolution because of their  
 33 feedback on the miscibility of CO<sub>2</sub> and on the density  
 34 gradients<sup>3,4</sup> and hence on the buoyancy-driven mixing.  
 35 Reaction products may also influence surface tension gradients  
 36 at the partially miscible interface and thus trigger Marangoni  
 37 flows. Such phenomena are difficult to explore in situ, and  
 38 simple model systems on which fundamental experimental  
 39 studies can be performed are needed.

40 Investigations of such interfacial hydrodynamic instabilities  
 41 have up to now been mainly focused on either fully miscible or  
 42 totally immiscible two-layer systems. In miscible systems,  
 43 Rayleigh–Taylor and double-diffusive instabilities have long  
 44 been known to affect stratification of nonreactive fluids in the  
 45 gravity field.<sup>5</sup> For reactive systems, convective dynamics have  
 46 also been experimentally and theoretically studied,<sup>6</sup> showing  
 47 how the reaction can severely change the symmetry of  
 48 convective modes.<sup>7</sup> Nonreactive double-layer miscible systems  
 49 with nonideal mixing properties have also been proposed to  
 50 mimic supercritical CO<sub>2</sub> dynamics at the interface with

51 aquifers.<sup>8,9</sup> However, the studies of such miscible interfaces  
 52 can only address buoyancy-driven convection and cannot take  
 53 into account the influence of partial miscibility and surface  
 54 tension effects on convective instabilities and transport  
 55 phenomena.

56 In parallel, in immiscible two-layer systems, coupling of  
 57 reactions with buoyancy- and Marangoni-driven instabilities is  
 58 responsible for a variety of patterns and complex spatiotem-  
 59 poral dynamics including oscillations and interfacial turbu-  
 60 lence.<sup>10–14</sup> Typically, these systems consist of two layers of  
 61 one or more solutes diffusing from one solvent to the other  
 62 provides the engine for chemical processes as well as density  
 63 and surface tension gradients at the origin of convective  
 64 motions.<sup>17</sup> Convection can develop in both phases, and chemo-  
 65 hydrodynamic processes are eventually dominated by a  
 66 diffusion-limited regime.<sup>18</sup> Immiscible systems lack thus the  
 67 specificity of partially miscible systems, which is a constant  
 68 feeding of reaction–diffusion–convection (RDC) dynamics  
 69 thanks to the one-way-directed transfer of matter from the  
 70 infinite reservoir of one pure liquid phase toward the “host”  
 71 one, governed by a solubilization process. In that case,  
 72 buoyancy- and Marangoni-driven convective motions can  
 73 maintain a strong feedback with the mass transfer rate.<sup>19</sup>  
 74 When a chemical reaction impacts the solubilization kinetics,  
 75

**Received:** January 8, 2014

**Accepted:** February 7, 2014

76 the chemical environment and physics of the system also  
77 change in time, further affecting the stability between the two  
78 layers.<sup>20,21</sup> Despite the interest for CO<sub>2</sub> sequestration and other  
79 applications,<sup>22,23</sup> studies and classification of RDC dynamics  
80 around spatially extended partially miscible interfaces are  
81 however missing.

82 In this Letter, we introduce the partially miscible  
83 stratification of an ester on top of a denser aqueous solution  
84 in a quasi-two-dimensional reactor as a rich laboratory-scale  
85 model system for experimental and theoretical studies of  
86 chemo-hydrodynamic instabilities at the interface between two  
87 partially miscible liquids. We also demonstrate how chemical  
88 reactions in the aqueous phase allow for a direct control of the  
89 hydrodynamic instabilities. This system features all specific  
90 characteristics of spatiotemporal convective dynamics in  
91 partially miscible systems and of their dependence on the  
92 miscibility, the solubilization kinetics, and chemical trans-  
93 formations.

94 Alkyl formates are organic ester compounds of general  
95 formula HCOOR', where R' is an alkyl chain. They are partially  
96 miscible in water with a solubilization constant of  $\chi_e = e_o/e_{(org)}$ ,  
97 where  $e_o$  and  $e_{(org)}$  represent the dimensional concentration of  
98 the alkyl formate in the saturated water phase and the  
99 dimensional pure ester concentration in the organic phase,  
100 respectively (see Table 1 and ref 24). In water, alkyl formates

**Table 1. Values of the Experimental Parameters for Three Alkyl Formates, HCOOR', with Increasing Alkyl Chain<sup>a</sup>**

alkyl chain (R')	$\rho_e$ at 20 °C (g cm <sup>-3</sup> )	$(1/\rho_w)(\partial\rho/\partial e)$ (M <sup>-1</sup> )	$\chi_e^{24}$ (%)
methyl- (-CH <sub>3</sub> )	0.974	0.0060 ± 0.0005	30
ethyl- (-CH <sub>2</sub> CH <sub>3</sub> )	0.921	0.0020 ± 0.0010	10
propyl- (-CH <sub>2</sub> CH <sub>2</sub> CH <sub>3</sub> )	0.904	na	0.2

<sup>a</sup> $\rho_w = 0.9982$  g cm<sup>-3</sup> is the pure water density at 20 °C.

101 undergo a slow spontaneous hydrolysis in neutral conditions to  
102 produce formic acid, HCOOH, and the alcohol, R'OH. The  
103 kinetics of the hydrolysis process is autocatalytic in acidic  
104 conditions<sup>25</sup> and is also considerably accelerated in an alkaline  
105 environment.<sup>26</sup> In aqueous solutions of alkaline hydroxides  
106 (MOH), the ester reacts with the base to yield a formate salt  
107 (HCOOM) and an alcohol (R'OH), according to the scheme



109 where M stands for the metal counterion of OH<sup>-</sup>. We study the  
110 chemo-hydrodynamic properties of the ester/water system in a  
111 quasi-two-dimensional geometry, where the less dense pure  
112 ester phase is set on top of the denser aqueous layer in the  
113 gravity field. The experimental setup consists of a Hele–Shaw  
114 cell made of two borosilicate glass plates separated by a thin  
115 polymer mask giving a gap width of 1 mm.<sup>27</sup> The dynamics in  
116 the colorless solutions is followed by an optical phase-shifting  
117 Schlieren technique<sup>28,29</sup> visualizing the variations in space and  
118 time of the refractive index, which are related to the density  
119 gradients inside of the solutions. All experimental images have a  
120 field of view of 2 cm × 2 cm. Reagent-grade reactants (Sigma-  
121 Aldrich) are used without further purification.

122 The typical convective instability observed with a short alkyl  
123 chain formate (methyl formate) is shown in Figure 1a; starting

from a buoyantly stable configuration, a hydrodynamic density  
fingering instability develops below the interface upon  
dissolution of pure methyl formate in the denser pure water.  
Here, the hydrolysis process is extremely slow with respect to  
the time scale at which the hydrodynamic instability occurs, and  
convective motions are induced by the local accumulation of  
the dissolved ester, HCOOCH<sub>3(aq)</sub>, just below the contact line  
between the aqueous and the organic phases. The convective  
dynamics is localized in the aqueous layer. Convective flows  
further enhance the solubilization of the ester in the water  
phase, thus feeding the instability similarly to what is observed  
in convective dissolution of CO<sub>2</sub> in water.<sup>1</sup> Once the fingers  
appear, they grow along the gravitational field, but they also  
exhibit a slow horizontal drift from the center to the borders of  
the cell (and vice versa), forming preferential hydrodynamic  
paths where fingers merge and persist in time (see also Figure  
1c). As the formate dissolves into the water, the interface not  
only tends to move upward, it also ripples and exhibits the  
formation of soliton-like horizontal waves, reminiscent of  
dissipative waves observed at the surface of liquids in  
Marangoni-driven flows.<sup>15,16</sup> The presence of an interfacial  
Marangoni contribution to the flow can be attributed here to  
the ester transfer into water and to the slow production of the  
alcohol that, even in traces, can induce strong surface activity.<sup>17</sup>  
In order to check the relative weight in the convective flows of  
vertical buoyancy-driven motions versus horizontal Marangoni  
flows close to the interface, we performed analogous experi-  
ments with the cell perpendicularly oriented with respect to the  
gravitational field. With this horizontal configuration, no  
convective motions could be detected, indicating that, contra-  
rily to the buoyancy-induced flows, Marangoni-driven con-  
vection is not suitable by itself to initiate the solubilization  
process and, thus, can be considered as a side effect also in the  
phenomenology of vertical experiments carried out in neutral  
conditions.

When the top layer is ethyl formate or propyl formate,  
buoyancy-driven fingering is also observed (Figure 1b,c). As for  
the methyl formate, convective dissolution is here dominated  
by the solubilization process rather than by the hydrolysis  
reaction. Comparing Figure 1a–c, we see that the system is less  
unstable when the length of the alkyl chain R' increases as less  
fingers appear and as they grow on a longer time scale. In the  
case of propyl formate/water, we observe just one finger  
emerging over a time scale 1 order of magnitude slower with  
respect to the methyl formate/water stratification. In the  
space–time plot of Figure 1c (right panel), we can appreciate  
the convective dynamics in which the fingers travel horizontally  
along the contact line, with a speed comparable to the slow  
vertical development. The instability growth rate follows the  
tendency of these esters to mix in water as convection develops  
more vigorously for shorter alkyl formates that are more  
miscible in water. However, it is opposite to the reactivity that,  
according to kinetic investigations,<sup>25</sup> increases with the alkyl  
chain length.

The relative importance of the miscibility and of the  
reactivity of the ester in the convective dissolution dynamics  
can be rationalized by means of a minimal model in which the  
solubilization and reactive processes are coupled with the  
Stokes equations, governing the evolution of the velocity field  $\mathbf{v}$   
 $= (u, v)^T$  in the reactor. We consider a two-dimensional vertical  
slab in a reference frame  $(x, z)$ , in which the gravitational vector  
 $\mathbf{g}$  is oriented against the vertical direction  $z$ . Because the upper  
organic phase is not affected by the hydrodynamic flows, we

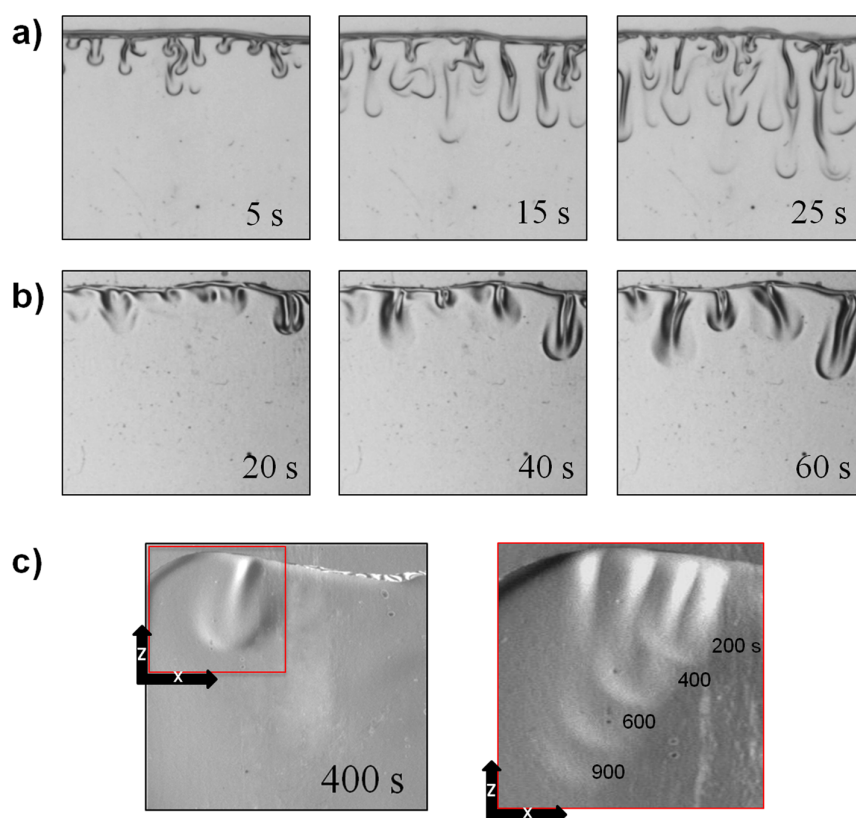


**Figure 1.** Typical density fingering observed experimentally below the horizontal interface between pure water and pure methyl formate (a), ethyl formate, (b) and propyl formate (c). The ester lies on top of the aqueous phase. In (c), the space–time plot in the right panel follows at successive times the vertical growth and the horizontal drifting of the finger shown in the left panel within the red frame (field of view  $0.95 \text{ cm} \times 0.95 \text{ cm}$ ).

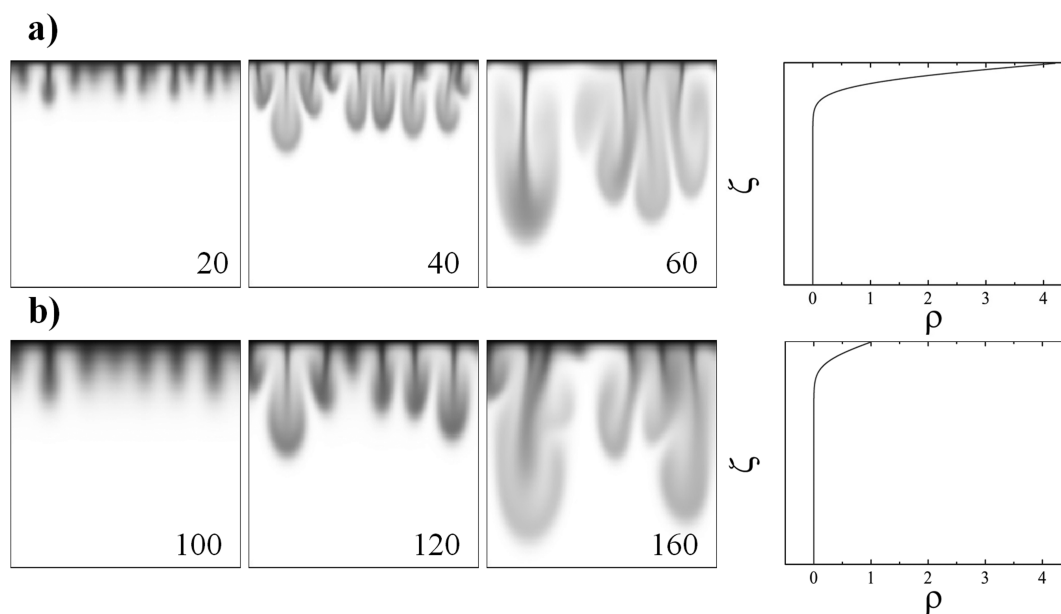


**Figure 2.** Spatiotemporal dynamics of the ester concentration computed numerically for the nonreactive convective dissolution of methyl formate/water (a) and ethyl formate/water (b) stratification. The last snapshot of each row shows the asymptotic dimensionless density profile ( $R_e = 1$ ), which has a self-similar form in the rescaled variable  $\zeta = z/(D_e t)^{1/2}$ . To emphasize the difference in the density profile of the two systems, concentration values are scaled over the ethyl formate concentration in the saturated water phase. The spatial domain of numerical simulations is  $1 \text{ cm}^2$ .

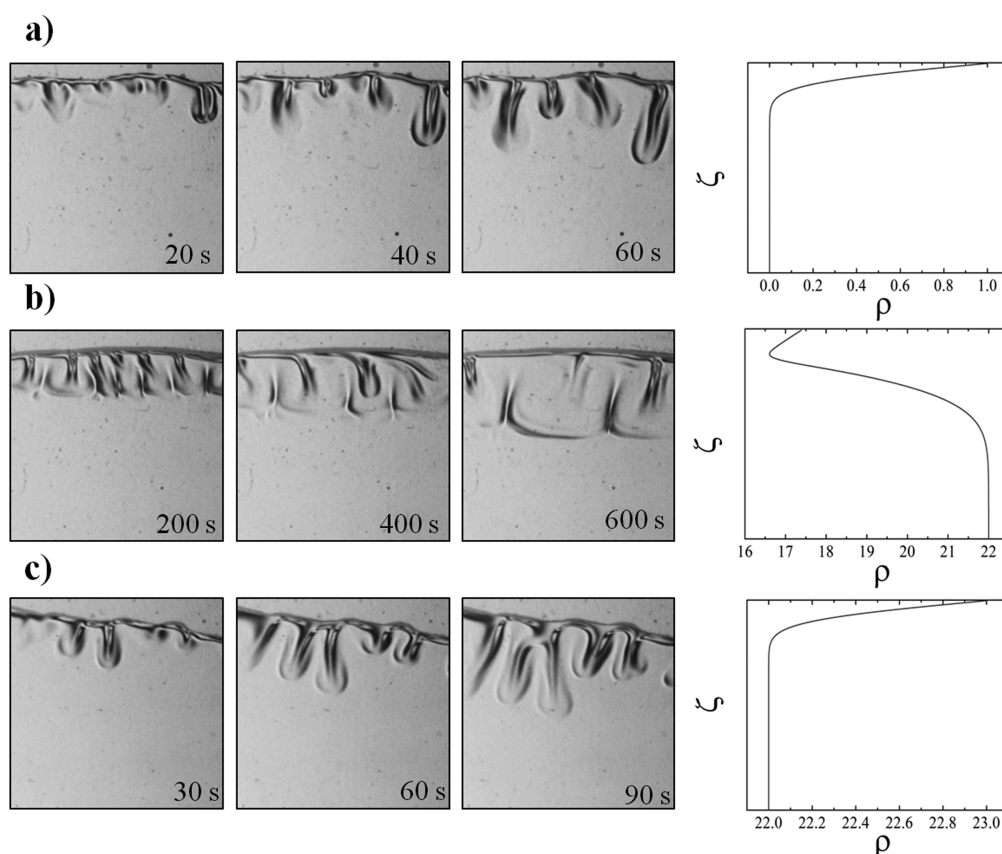


**Figure 3.** Experimental spatiotemporal dynamics below of the interface between ethyl formate and (a) pure water, (b) 1 M NaOH solution, and (c) 1.07 M NaCl solution. In the (b) and (c), the aqueous solutions have the same initial density. The last snapshot of each row shows the asymptotic density profile computed numerically, as described in the text by using  $R_{\text{HCOOEt}} = 1.0$ ,  $R_{\text{NaOH}} \approx 22.0$ ,  $R_{\text{HCOONa}} = 20.5$ , and  $R_{\text{EtOH}} = -4.1$ .

187 focus our description on the bottom aqueous layer of width  $L_x$   
 188 and height  $L_z$ . Moreover, as the upward drifting of the interface  
 189 is negligible on the hydrodynamic time scale, the reference  
 190 frame is kept fixed. No-slip boundary conditions are imposed to  
 191 the velocity field, and no-flux at all boundaries are used for all  
 192 concentrations except that at the top where we take a constant  
 193 value  $e_o$  boundary condition for the ester. This mimics the  
 194 constant amount of formate solubilizing at the interface from  
 195 the upper phase, which, under the hypothesis of local  
 196 equilibrium, is given by the solubility  $e_o = e|_{L_z} = \chi_e e_{(\text{org})}$ .<sup>30</sup>  
 197 The dimensionless RDC equations<sup>6,31</sup> are written in the  
 198 Boussinesq approximation and in the vorticity-stream function  
 199  $(\omega - \psi)$  form

$$\frac{\partial c_i}{\partial t} + \left( \frac{\partial \psi}{\partial z} \frac{\partial c_i}{\partial x} - \frac{\partial \psi}{\partial x} \frac{\partial c_i}{\partial z} \right) = \delta_i \nabla^2 c_i + \mathcal{D} f_i$$

200  $\forall$   $i$ th chemical species (2)

$$\nabla^2 \omega = \sum_i R_i \frac{\partial c_i}{\partial x}$$

201 (3)

$$\frac{\partial^2 \psi}{\partial x^2} + \frac{\partial^2 \psi}{\partial z^2} = -\omega$$

202 (4)

203 where the horizontal and the vertical components of the  
 204 velocity field are tied to the stream function through the  
 205 relations  $u = \partial_z \psi$  and  $v = -\partial_x \psi$ . The  $c_i$  indicates the

dimensionless aqueous concentration of the  $i$ th species, and  $f_i$  206  
 is the related chemical kinetics. In our description, we introduce 207  
 the Damköhler number  $\mathcal{D}$  as the ratio between the 208  
 hydrodynamic and the chemical time scales.<sup>31</sup> In neutral 209  
 conditions, the reactive process can be neglected with respect 210  
 to the hydrodynamic characteristic time scale (thus,  $\mathcal{D} \rightarrow 0$ ), 211  
 and the aqueous alkyl formate with dimensionless concen- 212  
 tration  $c_e$  is the only species ruling the system instability. The 213  
 second-order kinetics  $f_i = kc_e c_{\text{MOH}}$  describing reaction 1 comes 214  
 into play when we consider the alkaline hydrolysis. In this case, 215  
 the hydrodynamic and the chemical time scales are comparable 216  
 ( $\mathcal{D} \approx 1$ ), and the reaction products are also taken into account 217  
 in the model along with the ester and the base. For simplicity, 218  
 the diffusivity ratios  $\delta_i = D_i/D_e$  between each species diffusivity 219  
 $D_i$  and the ester diffusivity in water  $D_e$  are all taken equal to 220  
 unity. The buoyancy ratio  $R_i = (\partial \rho / \partial [i]) / (\partial \rho / \partial e)$  quantifies 221  
 the relative contribution of the  $i$ th species to the local 222  
 dimensionless density as 223

$$\rho(i) = \sum_i R_i c_i$$

(5) 224

As shown in Figure 2, the main dynamical features observed 225  
 experimentally for the different alkyl formates are well- 226  
 reproduced numerically and can be understood in terms of 227  
 the dimensionless asymptotic density profiles.<sup>6,7</sup> These are 228  
 derived by introducing in eq 5 the numerical asymptotic 229  
 concentration profiles of the pure reaction–diffusion problem 230

(eq 2) (with  $\psi = 0$ ) and the proper values for the buoyancy ratio  $R_i$  of each active chemical species as given in Figure 2. At long times ( $t \rightarrow \infty$ ), the reaction–diffusion solutions converge to a self-similar concentration profile in the rescaled variable  $\zeta = z/(D_e t)^{1/2}$ . In the nonreactive case, the density profiles in the aqueous layer (see the last snapshots in Figure 2) show a local maximum at the top of the water phase where the dissolving alkyl formate produces a mass accumulation with respect to the bottom region. The density jump decreases as the alkyl chain length becomes longer, that is, when the decrease in solubility leads to a smaller density jump. As supported by the numerical simulations in Figure 2, the effect is that the less soluble ester (Figure 2b) produces a smaller density jump below the interface and hence slow-growing fingers while the instability readily develops with the more soluble methyl formate (Figure 2a). Both experimental and numerical evidence lead us to propose the solubilization constant of an ester,  $\chi_e$ , as the main parameter influencing the density jump at the interface in nonreactive conditions and, hence, the onset time and the strength of the convective instability. In the modeling, this dependence on  $\chi_e$  (and on  $e_{(\text{org})}$ ) explicitly appears in the characteristic hydrodynamic time and spatial scales  $t_h$  and  $L_h$ .<sup>31</sup>

Control of the convective instabilities in this ester/water two-layer system can be achieved by tuning the density profile (i) by changing ad hoc the density profile of the aqueous solution (through local changes in temperature for instance<sup>33</sup>), (ii) by influencing ad hoc the ester solubilization through a suitable change of the chemical or physical environment in the aqueous layer (via the addition of an inert compound, for instance, or a change of the global temperature), and/or (iii) promoting in situ changes of type (i) and (ii) through a chemical reaction.

To demonstrate experimentally the efficiency of the scenario where chemistry strongly modifies the hydrodynamic instability, we analyze spatiotemporal dynamics of a reactive case when the hydrolysis process is catalyzed by a base, as in reaction 1. Solutions of NaOH are used in the lower layer, and the concentration of the alkaline solute is varied in the range if [0.01, 2.00] M. Figure 3 compares the nonreactive solubilization of ethyl formate in pure water (Figure 3a) with the reactive one in NaOH (Figure 3b). We observe, thanks to the reaction, a strong stabilization of fingering that develops at the same vertical extent as that in Figure 3a but on a much longer time scale. This is related to the fact that the solutal expansion coefficient of the sodium formate produced by the hydrolysis reaction (its contribution to the density has been measured to be  $(1/\rho_w)/(\partial\rho/\partial[\text{HCOONa}]) = 0.0410 \pm 0.0005 \text{ M}^{-1}$ ) is smaller than that of the base ( $(1/\rho_w)/(\partial\rho/\partial[\text{NaOH}]) = 0.044 \text{ M}^{-1}$ ; see ref 32). The formation upon reaction of alcohol also decreases the local density of the medium ( $(1/\rho_w)/(\partial\rho/\partial[\text{EtOH}]) = 0.0081 \text{ M}^{-1}$ ; see ref 32). The result is that if the initial amount of base is large enough to transform a significant part of aqueous alkyl formate into the related less dense salt and the alcohol, a nonmonotonic density distribution with a depletion zone below the interface develops along the gravity field (see the last snapshot in Figure 3b). This density minimum features a stabilizing barrier that refrains from the fingering growth. Note that relative changes in density as small as  $10^{-3}$  are already sufficient to trigger macroscopic convective motions in a few seconds.<sup>6,7</sup> Depending upon the relative contribution of the reactants and products to the total density, the fingering arising from a solubilization mechanism can thus be controlled by a reaction. In the case of a nonmonotonic density profile with a minimum like that in the case discussed

above, convective patterns are prevented from developing downward. On the contrary, convective dissolution can be enhanced if the density profile remains monotonic and the density maximum at the interface is intensified by the chemical process.

In Figure 4a, the stabilizing effect experienced in the alkaline hydrolysis is quantified as a function of the concentration of the

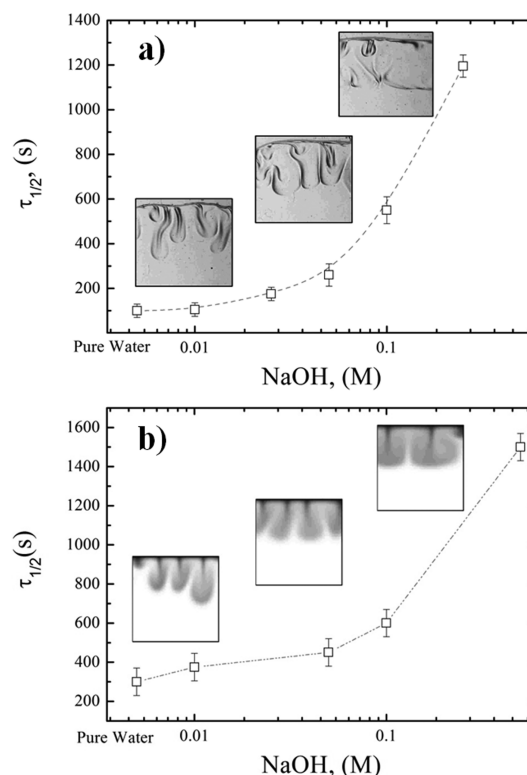


**Figure 4.** Experimental (a) and numerical (b) characteristic time  $\tau_{1/2}$  of the fingers growth as a function of the alkaline concentration of the aqueous phase.

base by computing  $\tau_{1/2}$ , the time required for the fingers to reach the mid length of the aqueous layer. This observable embeds average information on the fingering growth rate. The  $\tau_{1/2}$  values reported for each concentration point are averaged over six experiments, and the typical patterns obtained are also shown. There is an initial concentration domain where the dynamics is unaffected by the alkaline hydrolysis. For concentrations larger than  $[\text{NaOH}] = 0.1 \text{ M}$ , the system undergoes an increase in  $\tau_{1/2}$ . The slowing down of the instability goes along with a change in the finger's shape, which turns into "fatter" structures due to the dynamical formation of a minimum in the density profile (Figure 3b). The width of the fingers becomes larger as the alkaline solute concentration is increased and, typically, squared cells developing for  $[\text{NaOH}]$  larger than 1 M merge into a homogeneous stratification. It is worth remarking here that the control of the instability is completely governed by solutal density changes due to the reaction. Thermal contributions are negligible<sup>34</sup> while the shift of the aqueous solution density toward larger values is not able to induce the same effect on the finger growth and/or analogous patterns as a minimum in density. This can be verified by comparing the snapshots of Figure 3b and c, which

323 show isopycnic aqueous phases but feature an alkaline and a  
324 neutral environment, respectively. When the inert salt NaCl is  
325 added (Figure 3c), regular fingers with a faster characteristic  
326 time scale and a morphology comparable to those of the pure  
327 water case develop. This is because the density profile (even if  
328 shifted toward larger values by a constant due to the addition of  
329 NaCl) remains monotonically decreasing, that is, does not have  
330 the stabilizing minimum induced by the reaction with a base.  
331 The slight delay in the formation of the fingers with NaCl  
332 (Figure 3c) with regard to the neutral case (Figure 3a) might  
333 be due to an influence of NaCl on the solubility of the ester in  
334 the water, but this has not been quantified here. The trend and  
335 the patterns obtained by numerical integration of eqs 2–4, with  
336 the second-order kinetics of reaction 1, show a good qualitative  
337 and quantitative agreement with the experimental results (see  
338 Figure 4b). In particular, numerical simulations support the  
339 idea that even if the alkaline conditions speed up the formation  
340 of the alcohol that acts as a strong surfactant, buoyancy effects  
341 dominate the convective dynamics observed in the experiments.  
342 To summarize, the hydrolysis of alkyl formates in a two-layer  
343 superposition of an ester on top of partially miscible denser  
344 water in the gravitational field is proposed as a model system to  
345 study hydrodynamic instabilities of the interface between two  
346 partially miscible fluids. Buoyancy-driven fingering occurs,  
347 driven by the solubilization process of the ester into the  
348 water layer. The degree of solubility of the ester in the water is  
349 a key parameter controlling the onset time and the intensity of  
350 the convective dissolution instability in nonreactive conditions,  
351 while the influence of the hydrolysis of the ester in the water  
352 has a secondary effect in neutral conditions. Changing the  
353 chemical composition of the aqueous solution allows one to  
354 achieve a chemical control on the instability by tuning the  
355 density profile in the water phase. As an example, a chemical  
356 reaction of the ester with an alkaline hydroxide in the aqueous  
357 solution can induce a depletion zone below the interfacial  
358 region thanks to the in situ formation of a less dense salt. The  
359 result is that the density profile becomes nonmonotonic, and  
360 the finger growth is refrained from or even substituted by a  
361 stable stratification. New chemo-hydrodynamic scenarios could  
362 be induced by the nonlinear interplay between chemical  
363 kinetics and more complicated solubilization mechanisms (see,  
364 for instance, ref 35). This work shows, among others, that an  
365 understanding of the impact of chemical reactions on  
366 convective dissolution and trapping processes, which are  
367 important in applied problems as complex as CO<sub>2</sub> sequestra-  
368 tion, is a prerequisite to assess the optimal transport and  
369 dissolution conditions in partially miscible systems.

## 370 ■ AUTHOR INFORMATION

### 371 Corresponding Author

372 \*E-mail: mabudroni@uniss.it.

### 373 Present Address

374 <sup>§</sup>M.A.B.: Department of Chemistry and Pharmacy, University  
375 of Sassari, Via Vienna 2, Sassari 07100, Italy.

### 376 Notes

377 The authors declare no competing financial interest.

## 378 ■ ACKNOWLEDGMENTS

379 We acknowledge financial support from Prodex (M.A.B., L.L.,  
380 and A.D.), ARC CONVINCERE (A.D.), FNRS FORECAST  
381 (A.D.), Regione Sardegna POR project (M.A.B. and M.R.), the

ITN-Marie Curie-Multiflow network (L.A.R. and A.D.), and  
382 FRIA (L.L.). 383

## 384 ■ REFERENCES

- (1) Kneafsey, T. J.; Pruess, K. Laboratory Flow Experiments for  
385 Visualizing Carbon Dioxide-Induced Density-Driven Brine Con-  
386 vection. *Transp. Porous Media* **2010**, *3*, 123–139. 387
- (2) Kneafsey, T. J.; Pruess, K. Laboratory Experiments and  
388 Numerical Simulation Studies of Convectively Enhanced Carbon  
389 Dioxide Dissolution. *Energy Procedia* **2011**, *4*, 5114–5121. 390
- (3) Ennis-King, J.; Paterson, L. Coupling of Geochemical Reactions  
391 and Convective Mixing in the Long-Term Geological Storage of  
392 Carbon Dioxide. *Int. J. Greenhouse Gas Control* **2007**, *1*, 86–93. 393
- (4) Andres, J. T. H.; Cardoso, S. S. S. Onset of Convection in a  
394 Porous Medium in the Presence of Chemical Reaction. *Phys. Rev. E*  
395 **2011**, *83*, 046312. 396
- (5) Carballido-Landeira, J.; Trevelyan, P. M. J.; Almarcha, C.; De Wit,  
397 A. Mixed-Mode Instability of a Miscible Interface Due to Coupling  
398 Between Rayleigh–Taylor and Double-Diffusive Convective Modes.  
399 *Phys. Fluids* **2013**, *25*, 024107. 400
- (6) Almarcha, C.; Trevelyan, P. M. J.; Grosfils, P.; De Wit, A.  
401 Chemically Driven Hydrodynamic Instabilities. *Phys. Rev. Lett.* **2010**,  
402 *104*, 044501. 403
- (7) Lemaigre, L.; Budroni, M. A.; Riolfi, L. A.; Grosfils, P.; De Wit,  
404 A. Asymmetric Rayleigh–Taylor and Double-Diffusive Fingers in  
405 Reactive Systems. *Phys. Fluids* **2013**, *25*, 014103. 406
- (8) Backhaus, S.; Turitsyn, K.; Ecke, R. E. Convective Instability and  
407 Mass Transport of Diffusion Layers in a Hele–Shaw Geometry. *Phys.*  
408 *Rev. Lett.* **2011**, *106*, 104501. 409
- (9) Neufeld, J. A.; Hesse, M. A.; Riaz, A.; Hallworth, M. A.; Tchelepi,  
410 H. A.; Huppert, H. E. Convective Dissolution of Carbon Dioxide in  
411 Saline Aquifers. *Geophys. Res. Lett.* **2010**, *37*, L22404. 412
- (10) Sherwood, T. S.; Wei, J. C. Interfacial Phenomena in Liquid  
413 Extraction. *Ind. Eng. Chem.* **1957**, *49*, 1030–1034. 414
- (11) Eckert, K.; Grahn, A. Plumes and Finger Regimes Driven by an  
415 Exothermic Interfacial Reaction. *Phys. Rev. Lett.* **1999**, *82*, 4436–4439. 416
- (12) Eckert, K.; Acker, M.; Shi, Y. Chemical Pattern Formation  
417 Driven by a Neutralization Reaction. Part I: Mechanism and Basic  
418 Features. *Phys. Fluids* **2004**, *16*, 385–399. 419
- (13) Shi, Y.; Eckert, K. Orientation-Dependent Hydrodynamic  
420 Instabilities from Chemo-Marangoni Cells to Large Scale Interfacial  
421 Deformations. *Chin. J. Chem. Eng.* **2007**, *15*, 748–753. 422
- (14) Eckert, K.; Acker, M.; Tadmouri, R.; Pimienta, V. Chemo-  
423 Marangoni Convection Driven by an Interfacial Reaction: Pattern  
424 Formation and Kinetics. *Chaos* **2012**, *22*, 037112. 425
- (15) Weidman, P. D.; Linde, H.; Velarde, M. G. Evidence for Solitary  
426 Wave Behavior in Marangoni–Bénard Convection. *Phys. Fluids A*  
427 **1992**, *4*, 921–926. 428
- (16) Schwarzenberger, K.; Köllner, T.; Linde, H.; Odenbach, S.;  
429 Boeck, T.; Eckert, K. On the Transition from Cellular to Wavelike  
430 Patterns during Solutal Marangoni Convection. *Eur. Phys. J.: Spec. Top.*  
431 **2013**, *219*, 121–130. 432
- (17) Sternling, C. V.; Scriven, L. E. Interfacial Turbulence:  
433 Hydrodynamic Instability and the Marangoni Effect. *AIChE J.* **1959**,  
434 *4*, 514–523. 435
- (18) Lavabre, D.; Pradines, V.; Micheau, J.-C.; Pimienta, V. Periodic  
436 Marangoni Instability in Surfactant (CTAB) Liquid/Liquid Mass  
437 Transfer. *J. Phys. Chem. B* **2005**, *109*, 7582–7586. 438
- (19) Mendes-Tassis, M. A.; Perez de Ortiz, E. S. Spontaneous  
439 Interfacial Convection in Liquid–Liquid Binary Systems Under  
440 Microgravity. *Proc. R. Soc. London* **1992**, *438*, 389–396. 441
- (20) Perez de Ortiz, E. S.; Sawistowski, H. Interfacial Stability of  
442 Binary Liquid–Liquid Systems-II. Stability Behavior of Selected  
443 Systems. *Chem. Eng. Sci.* **1973**, *28*, 2063–2069. 444
- (21) Agble, D.; Mendes-Tassis, M. A. The Effect of Surfactants on  
445 Interfacial Mass Transfer in Binary Liquid–Liquid Systems. *Int. J. Heat*  
446 *Mass Transfer* **2000**, *43*, 1025–1034. 447

- 448 (22) Citri, O.; Kagan, M. L.; Kosloff, R.; Avnir, D. The Evolution of  
449 Chemically Induced Unstable Density Gradients Near Horizontal  
450 Reactive Interfaces. *Langmuir* **1990**, *6*, 559–564.
- 451 (23) Savino, R.; Lappa, M. Dissolution and Solutal Convection in  
452 Partially Miscible Liquid Systems. *Int. J. Heat Mass Transfer* **2004**, *47*,  
453 601–612.
- 454 (24) Góral, M.; Shaw, D. G.; Maczyński, A.; Wiśniewska-Gocłowska,  
455 B.; Jeziernski, A. IUPAC–NIST Solubility Data Series. 88. Esters with  
456 Water-Revised and Updated. Part 1. C<sub>2</sub> to C<sub>4</sub> Esters. *J. Phys. Chem. Ref.*  
457 *Data* **2009**, *38*, 1093–1127.
- 458 (25) Jogunola, O.; Salmi, T.; Eranen, K.; Warna, J.; Kangas, M.;  
459 Mikkola, J. P. Reversible Autocatalytic Hydrolysis of Alkyl Formate:  
460 Kinetic and Reactor Modeling. *Ind. Eng. Chem. Res.* **2010**, *49*, 4099–  
461 4106.
- 462 (26) Patai, S. *The Chemistry of Carboxylic Acids and Esters*; John Wiley  
463 and Sons Ltd: Chichester, New York, Brisbane, Toronto, 1969.
- 464 (27) Shi, Y.; Eckert, K. A Novel Hele–Shaw Cell Design for the  
465 Analysis of Hydrodynamic Instabilities in Liquid–Liquid Systems.  
466 *Chem. Eng. Sci.* **2008**, *63*, 3560–3563.
- 467 (28) Settles, G. S. *Schlieren and Shadowgraph Techniques*; Springer:  
468 Berlin, Heidelberg, Germany; New York, 2001.
- 469 (29) Joannes, L.; Dubois, F.; Legros, J.-C. Phase-Shifting Schlieren:  
470 High-Resolution Quantitative Schlieren that Uses the Phase-Shifting  
471 Technique principle. *Appl. Opt.* **2003**, *42*, 5046–5053.
- 472 (30) These values are calculated as  $e = \chi_e e_{(\text{org})}$ , where  $e_{(\text{org})} = 15$  M for  
473 the methyl formate and 12 M for the ethyl formate. If needed, the  
474 boundary condition could involve a functional dependence of  $\chi_e$  on  
475 the concentration of the chemical species in order to describe the  
476 dynamical feedback of the reaction on the solubility of the ester in the  
477 water (see ref 35).
- 478 (31) The concentrations, velocity field, spatial domain, and time are  
479 nondimensionalized by  $e_o$ ,  $u_h = gK\alpha_e e_o/\nu$ ,  $l_h = D_e/u_h$ , and  $t_h = D_e/u_h^2$ ,  
480 respectively, where  $\alpha_e = (1/\rho_w)(\partial\rho/\partial e)$  is the solutal expansion  
481 coefficient of the solubilized ester,  $g$  is the magnitude of the  
482 gravitational acceleration,  $\nu$  and  $\rho_w$  are the kinematic viscosity and  
483 the density of water, respectively, and  $D_e$  is the diffusivity of the alkyl  
484 formate in the aqueous medium ( $\sim 10^{-8}$  cm<sup>2</sup> s<sup>-1</sup>).  $K$  is the  
485 permeability, equal to  $a^2/12$  for a Hele–Shaw cell with a gap width  
486 of  $a$ . The pressure scale is defined as  $p_a + \rho_w g z + \mu D_e/K$ , where  $p_a$   
487 denotes the ambient pressure and  $\mu = \nu\rho_w$  is the water dynamic  
488 viscosity. The Damköhler number is defined as  $\mathcal{D} = t_h k e_o$ , where  $k$  is  
489 the kinetic constant of the ester hydrolysis and  $1/(k e_o)$  defines the  
490 chemical time scale.
- 491 (32) *CRC Handbook of Chemistry and Physics*, 56th ed.; CRC Press:  
492 Cleveland, OH; 1975–1976.
- 493 (33) Bratsun, D. A.; Shi, Y.; Eckert, K.; De Wit, A. Control of  
494 Chemo-Hydrodynamic Pattern Formation by External Localized  
495 Cooling. *Europhys. Lett.* **2005**, *69*, 746–752.
- 496 (34) Almarcha, C.; Trevelyan, P. M. J.; Grosfils, P.; De Wit, A.  
497 Thermal Effects on the Diffusive Layer Convection Instability of an  
498 Exothermic Acid–Base Reaction Front. *Phys. Rev. E* **2013**, *88*, 033009.
- 499 (35) Roque, C.; Pimienta, V.; Lavabre, D.; Micheau, J. C.  
500 Solubilization Processes in Autocatalytic Biphasic Reactions. *Langmuir*  
501 **2000**, *16*, 6492–6496.